J. Fluid Mech. (1982), *vol.* 120, *pp.* 359–383
Printed in Great Britain

The effects of obstacle shape and viscosity in deep rotating flow over finite-height topography

By E. R. JOHNSON
Department of Mathematics, University College London

(Received 26 November 1980 and in revised form 30 December 1981)

The limiting process introduced by Stewartson & Cheng (1979) is used to obtain solutions in the limit of vanishing Rossby number for deep rotating flows at arbitrary Reynolds number over cross-stream ridges of finite slope. Examination of inviscid solutions for infinite-depth flow shows strong dependence on obstacle shape of not only the magnitudes but also the positions of disturbances in the far field. In finite-depth flow there is present the Stewartson & Cheng inertial wave wake, which may be expressed as a sum of vertical modes whose amplitudes depend on the obstacle shape but are independent of distance downstream; the smoother the topography and the shallower the flow, the fewer the number of modes required to describe the motion. For abrupt topography the strength of the wake does not, however, decrease monotonically with decreasing container depth (or Rossby number). In very deep flows viscosity causes the wake to decay on a length scale of order the Reynolds number times the ridge width. In shallower flows, where only a few modes are present, the decay of the wake is more rapid. For Reynolds numbers and depths of the order of those in the experiments of Hide, Ibbetson & Lighthill (1968), viscosity causes the disturbance to take on the appearance of a leaning column.

1. Introduction

Steady, slow, horizontal motion of an obstacle in an inviscid homogeneous fluid rotating rapidly about a vertical axis sets up a motion whose scale of vertical variation is much greater than other length scales in the problem. Lighthill (1967) points out that either viscous (non-zero Ekman number E) or inertial (non-zero Rossby number Ro) effects limit the extent of the disturbance in a deep container. For obstacles with a horizontal length scale l these effects introduce vertical scales in the motion of order respectively l/E and l/Ro (Hide, Ibbetson & Lighthill 1968; hereinafter referred to as HIL), whose ratio is the Reynolds number Re of the flow. If $Re \ll 1$, viscous effects dominate the vertical structure, and the motion is similar to that for a rising sphere in a rotating fluid, described by Moore & Saffman (1968, 1969) and Hocking, Moore & Walton (1979) for different limits of the ratio of container depth to l/E. If $Re \gg 1$ inertial effects dominate, and the motion may be described in terms of inertial wave radiation (Lighthill 1967).

Experiments (with $25 \lesssim Re \lesssim 150$) in containers sufficiently deep to show axial variations in the disturbance pattern are described by HIL, who note that the salient feature of the flow is a columnar disturbance above and behind an obstacle, tilted from the vertical by an angle proportional to Ro. Arguing from his theory of wave propagation in inviscid dispersive media, Lighthill, in the appendix to HIL, predicts such a

leaning column, and obtains a value for the constant of proportionality in close agreement with the value determined experimentally.

Inviscid flow is considered in greater detail by Cheng (1977), who discusses motion in infinitely deep containers, and by Stewartson & Cheng (1979; hereinafter referred to as SC), who present an asymptotic theory for vanishing Ro for containers of depth of order l/Ro. The solutions in SC consist of a countably infinite set of vertical modes, separated, in their discussion, into a depth-independent mode, which dominates the solution at smaller depths, and an inertial wave wake, which extends downstream with undiminishing amplitude. SC note that the absence of the wake in the experiments of HIL is due to the relatively large experimental viscosities, and point out the inapplicability of a purely inviscid description of the observed motion.

Mason & Sykes (1981) present further experimental observations and numerical integrations of the full three-dimensional Navier–Stokes equations at values of viscosity corresponding to those in the experiments. The integrations agree well with the observations, showing that, although the flow has the appearance of a leaning column, viscously damped inertial waves are also present. Mason & Sykes (1981) also present spatially periodic numerical solutions to linear viscous equations valid for obstacles of infinitesimal slope. These solutions relate closely to the numerical results at experimental viscosities provided the asymmetry in the latter due to vortex stretching is ignored.

The flow may be regarded as a dispersive wave field propagating away from an obstacle where, through nonlinear processes, it is generated. The purpose of the present work is to give a simple physical situation in which analytic solutions may be obtained for flows of arbitrary viscosity over finite-height topography of various shapes. In the flows considered here the wave-generation process is linear, so the energy spectrum of the forcing is known and the effects of obstacle shape and viscosities ranging from zero to the relatively large experimental values may be discussed.

In § 2 the limiting process introduced by SC is used to derive the zero-Ro nonlinear equations of motion for topography of finite slope in flow of arbitrary depth, retaining viscous effects. The Reynolds number is finite, and so the vertical scales introduced by viscosity and inertial effects are comparable. For the special case of flow over ridge-like topography, the equations are linear even for finite-amplitude disturbances. The vertical flow field is insensitive to the boundary conditions on the flow at large cross-stream distances, although these affect the horizontal flow increasingly as the depth of the container is decreased.

In § 3 a container of infinite depth is considered. Solutions are presented for obstacles of compact and infinite support and of varying degrees of differentiability. Group-velocity arguments give an accurate description of the inviscid flow field, showing that although the maximum disturbance occurs along a straight line it cannot be associated with a columnar disturbance at heights greater than order l/Ro. The inviscid flow pattern depends strongly on the energy spectrum of the waves generated by the obstacle. At a fixed height, the amplitude of the wake decays with distance downstream at a rate governed by the rate of decay with increasing wavenumber of the excited wave spectrum. Thus a top-hat-profile wake decays algebraically, whilst a Gaussian-profile wake decays exponentially (and so has a distinctly columnar appearance).

The effect of viscosity is also strongly dependent on obstacle shape. Viscosity causes decay on a vertical length scale of order lEk_{m}^3 (where k_{m} is a representative obstacle

wavenumber), and also removes high-wavenumber contributions to the energy spectrum, attenuating the downstream wake on a length scale of order lRe and causing even the disturbance associated with a top-hat profile to appear columnar. The Gaussian profile, having little energy at high wavenumbers, is least affected by viscosity.

In §4 the effect of finite depth is considered. The flow consists of a viscously modified form of the inertial wave wake of SC and may be expressed as a countably infinite set of vertical modes. The amplitude of each mode is determined by the transform of the obstacle shape. For $H = hRo/l \gg 1$ (where h is the container depth) many modes are present, with amplitudes proportional to $H^{-\frac{1}{2}}$, the flow is closely described by reflection of radiated inertial waves, and viscosity causes decay on a horizontal length scale of order lRe. For $H \ll 1$, only the lowest modes are present and the flow decays on the shorter scale of $lH/(Re^{-1} + E^{\frac{1}{2}})$ due to the combined effects of internal dissipation and Ekman pumping.

The drag exerted on a submerged obstacle is calculated in §5. The drag estimates the strength of the wake, approaching a limiting value algebraically with increasing container depth and vanishing for isolated topography with decreasing depth. For topography with discontinuous slope, the drag assumes a significant fraction of its infinite-depth value even in quite shallow flows, and is not a monotonic function of depth. As noted by Mason & Sykes (1981), viscosity confines the disturbance to the neighbourhood of an obstacle, weakening reflection of inertial waves and causing the flow near the lower boundary to resemble more closely infinite-depth flow. The drag thus approaches its infinite-depth value in shallower flows when viscosity is included.

2. Governing equations

Consider an obstacle of horizontal scale l and height h_0 affixed to the lower boundary of an incompressible fluid of kinematic viscosity ν, depth h, confined between two horizontal planes and rotating with angular velocity Ω about a vertical axis. Suppose the undisturbed fluid velocity far from the obstacle is uniform and of magnitude U such that the Rossby number $Ro = U/2\Omega l$ is small. Take Cartesian axes $Ox^*y^*z^*$, with origin within the obstacle, Ox^* parallel to the unperturbed flow, and Oz^* vertical, with corresponding velocity components (u^*, v^*, w^*), and introduce non-dimensional variables

$$\left.\begin{aligned} &x = x^*/l, \quad y = y^*/l, \quad z = z^*/h, \quad t = t^*U/l, \\ &u = u^*/U, \quad v = v^*/U, \quad w = w^*/U, \quad p = (p^* - p_e^*)/2\rho U\Omega l, \end{aligned}\right\} \tag{2.1}$$

where $p^* - p_e^*$ gives the deviation of the pressure from its equilibrium value. The motion depends on three non-dimensional groups other than the Rossby number. These may be taken to be the obstacle slope $\alpha = h_0/l$, the Reynolds number $Re = Ul/\nu$ and the parameter introduced by SC, $H = hRo/l$, which is the ratio of the depth of the fluid to the vertical scale of inertial effects. The non-dimensional equations of motion are

$$u = -\frac{\partial p}{\partial y} - Ro(D_t v - Re^{-1}\nabla^2 v), \tag{2.2a}$$

$$v = \frac{\partial p}{\partial x} + Ro(D_t u - Re^{-1}\nabla^2 u), \tag{2.2b}$$

$$\frac{\partial p}{\partial z} = -H(D_t w - Re^{-1}\nabla^2 w), \tag{2.2c}$$

$$H\frac{\partial u}{\partial x} + H\frac{\partial v}{\partial y} + Ro\frac{\partial w}{\partial z} = 0, \tag{2.2d}$$

where $D_t = \partial_t + u\partial_x + v\partial_y + (Ro/H)w\partial_z$, and $\nabla^2 = \partial_x^2 + \partial_y^2 + (Ro/H)^2\partial_z^2 = \nabla_1^2 + (Ro/H)^2\partial_z^2$. The obstacle is taken to be $z^* = h_0 f(x, y)$, where f has maximum value unity, giving the conditions on the flow at solid boundaries as

$$u = v = w = 0 \quad \text{at} \quad z = \alpha H^{-1} Ro f \quad \text{and} \quad z = 1. \tag{2.3}$$

In the limit introduced by SC of vanishing Rossby number with H, Re and α fixed, (2.2) becomes

$$u = -\frac{\partial p}{\partial y}, \tag{2.4a}$$

$$v = \frac{\partial p}{\partial x}, \tag{2.4b}$$

$$\frac{\partial p}{\partial z} = -H\left[\frac{\partial w}{\partial t} + \frac{\partial(p, w)}{\partial(x, y)} - Re^{-1}\nabla_1^2 w\right], \tag{2.4c}$$

$$\frac{\partial w}{\partial z} = H\left[\frac{\partial}{\partial t}(\nabla_1^2 p) + \frac{\partial(p, \nabla_1^2 p)}{\partial(x, y)} - Re^{-1}\nabla_1^4 p\right]. \tag{2.4d}$$

This system retains the highest-order horizontal derivatives and so resolves vertical shear layers present above discontinuities in topographic slope. However, the highest-order vertical derivatives are absent, and thus the viscous boundary condition causes a thin boundary layer on non-vertical boundaries. This layer is the standard Ekman layer of dimensional thickness $(\nu/2\Omega)^{\frac{1}{2}}$. The layer thickness non-dimensionalized on the horizontal scale of the topography may be written as $E^{\frac{1}{2}}$, where $E = \nu/2\Omega l^2 = Ro/Re$ is an Ekman number for the flow. The boundary layer thus has thickness $O(Ro^{\frac{1}{2}}) \ll 1$, and forces an Ekman pumping modification to the vertical velocity which is also $O(Ro^{\frac{1}{2}})$. Since (2.4) is valid to $O(Ro)$ the pumping term is larger than any neglected term, and may be retained, although for α and H of order unity it is dominated by topographic forcing. It is noted later that for sufficiently small H, or sufficiently large Re, Ekman pumping can be the dominant dissipative effect. The boundary conditions on (2.4) are thus

$$w = \alpha\frac{\partial(p, f)}{\partial(x, y)} + E^{\frac{1}{2}}\nabla_1^2 p \quad \text{on} \quad z = 0, \tag{2.5a}$$

$$w = -E^{\frac{1}{2}}\nabla_1^2 p \quad \text{on} \quad z = 1, \tag{2.5b}$$

$$(p_x, p_y, p_z) = (0, -1, 0) \quad \text{as} \quad r \to \infty, \quad t < \infty. \tag{2.5c}$$

System (2.4), (2.5) is the viscous system corresponding to the weakly nonlinear system derived by SC, to which it reduces in the limit $Re \to \infty$. Involving no linearization about upstream conditions, it is valid for thick obstacles and arbitrary H. Ingersoll (1969) and Huppert (1975) have solved the inviscid system in the limit $\alpha \to 0$, $H \to 0$ with the Hide (1961) parameter α/H fixed, giving solutions where topographically generated velocities are of the same order as the upstream velocity. A different limit

of the system (2.2), (2.3) is the Queney (1947) limit: $\alpha \to 0$ with Ro and H fixed, discussed by Mason & Sykes (1981). This involves a linearization about upstream conditions, and so, although helpful in discussing some flow properties, is of limited use in the construction of finite-amplitude solutions, being valid solely for obstacles of infinitesimal slope for which topographically generated perturbations are dominated by the oncoming flow. The examination in SC of (2.4), (2.5) continues by expanding solutions to order α. This gives precisely the $Ro \to 0$ limit of the Queney system, and so for these equations, with H fixed, the operations of linearizing about upstream conditions and of letting $Ro \to 0$ commute.

For an obstacle which varies only slowly in the cross-stream direction, a solution of (2.4), (2.5) may be obtained for arbitrary α. Since this involves no linearization about upstream conditions it is not rigorously derivable by the Queney procedure. Consider an obstacle which for $|y| < L$ (where $L/l \sim Ro^{-1}$) is of constant cross-section, i.e. f is a function of x alone. We look for a solution of the form

$$w = w(x,z,t), \quad p = -y + \psi(x,z,t). \tag{2.6}$$

From (2.4), (2.5) and (2.6), the vertical velocity satisfies

$$\left\{H^2\left(\frac{\partial}{\partial t}+\mathscr{L}\right)^2 \frac{\partial^2}{\partial x^2}+\frac{\partial^2}{\partial z^2}\right\} w = 0, \tag{2.7a}$$

$$\left\{\left(\frac{\partial}{\partial t}+\mathscr{L}\right)-\mu\frac{\partial}{\partial z}\right\} w = \alpha\mathscr{L}\frac{\partial f}{\partial x} \quad \text{on} \quad z = 0, \tag{2.7b}$$

$$\left\{\left(\frac{\partial}{\partial t}+\mathscr{L}\right)+\mu\frac{\partial}{\partial z}\right\} w = 0 \quad \text{on} \quad z = 1, \tag{2.7c}$$

$$w \to 0 \quad \text{as} \quad r \to \infty, \quad t < \infty, \tag{2.7d}$$

where $\mathscr{L} = \partial/\partial x - Re^{-1}\partial^2/\partial x^2$, and $\mu = E^{\frac{1}{2}}/H$. The parameter μ may also be written in the form $E_{\mathrm{v}}^{\frac{1}{2}}/Ro$ where $E_{\mathrm{v}} = \nu/2\Omega h^2$ is an Ekman number based on the depth of the container. In this form it is seen that μ measures the ratio of viscous dissipation of vorticity by Ekman pumping to vortex compression by inertial effects. For H of order unity or greater, $\mu \sim Ro^{\frac{1}{2}}$, and Ekman pumping is a weak effect. However, for $h/l \sim Ro^{-\frac{1}{2}} \gg 1$ or smaller, $H \sim Ro^{\frac{1}{2}} \ll 1$, and Ekman pumping is a zeroth-order effect. This is considered in more detail in §4.

The superposition of a uniform velocity VU parallel to the ridge, i.e. taking $p = -y + Vx + \psi(x,z,t)$ in (2.6), does not affect (2.7); the vertical field is independent of the direction of approach of the oncoming flow, depending solely on the magnitude of the component normal to the ridge. Thus the vertical field may be regarded as the flow over the central portion of elongated isolated topography, as discussed in the limit $H \to 0$, α/H constant by Smith (1979), or as the flow over the central portion of a ridge bounded by side walls at $|y| = L \gg l$, as in the experiments of Boyer (1971*a*, *b*) and the theory of Huppert & Stern (1974). The precise form of the horizontal velocity field is important, however, in determining the drag on topography, and is considered in more detail in §5.

A convenient variable for comparison of analytic results for steady flows with experimental observations, like those of HIL and Mason & Sykes (1981), of dye released at various heights far upstream, is the deviation $l\zeta(x, z_\infty)$ of a fluid particle

from its upstream level hz_∞. The Lagrangian co-ordinate z_∞ is related in steady flow to the height $z(x, z_\infty)$ of the particle at position x through the Eulerian velocity field:

$$z(x, z_\infty) = z_\infty + H^{-1}Ro \int_{-\infty}^{x} \frac{w(\xi, z(\xi, z_\infty))}{u(\xi, z(\xi, z_\infty))} d\xi. \tag{2.8}$$

Thus z deviates from z_∞ by $O(Ro)$, and, to that order,

$$\frac{\partial \zeta}{\partial x}(x, z_\infty) = w(x, z) = w(x, z_\infty). \tag{2.9}$$

Substituting (2.8), (2.9) in (2.7) gives

$$H^2 \mathscr{L}^2 \frac{\partial^2 \zeta}{\partial x^2} + \frac{\partial^2 \zeta}{\partial z_\infty^2} = 0, \tag{2.10a}$$

$$\mathscr{L}\zeta - \mu \frac{\partial \zeta}{\partial z_\infty} = \alpha \mathscr{L} f \quad \text{on} \quad z_\infty = 0, \tag{2.10b}$$

$$\mathscr{L}\zeta + \mu \frac{\partial \zeta}{\partial z_\infty} = 0 \quad \text{on} \quad z_\infty = 1. \tag{2.10c}$$

For inviscid flow, $\zeta(x, 0) = \alpha f(x)$. The surface $z_\infty = 0$ coincides with the lower boundary of the fluid. In the co-ordinate system (x, z_∞) no transformation of the lower boundary condition is required, in contrast to the system (x, z), in which the boundary condition is transferred to $z = 0$.

It is assumed that solutions to (2.7) and (2.10) represent asymptotic forms correct to $O(Ro)$ of the solutions of the full equations of motion in the limit $Ro \to 0$. For fixed small Ro they are taken to approximate the flow field to order Ro. Plots of $hz_\infty + l\zeta(x, z_\infty)$ then approximate to $O(Ro)$ the projection of particle paths onto any plane $y =$ constant. In the following these are referred to, loosely, as particle paths. The approximation depends on vertical excursions of the fluid being small compared with either h or l/Ro, as opposed to the Queney linearization, which requires excursions to be small compared with l.

3. Very deep containers

When $H > 1$ and $Re > 1$ the smallest dynamically important vertical scale is l/Ro. In terms of $Z = z^*Ro/l = Hz$ the vertical velocity in steady flow satisfies

$$\left(\mathscr{L}^2 \frac{\partial^2}{\partial x^2} + \frac{\partial^2}{\partial Z^2}\right) w = 0, \tag{3.1a}$$

$$\left(\mathscr{L} - E^{\frac{1}{2}} \frac{\partial}{\partial Z}\right) w = \alpha \mathscr{L} \frac{\partial f}{\partial x} \quad \text{on} \quad Z = 0, \tag{3.1b}$$

$$\left(\mathscr{L} + E^{\frac{1}{2}} \frac{\partial}{\partial Z}\right) w = 0 \quad \text{on} \quad Z = H, \tag{3.1c}$$

$$w \to 0 \quad \text{as} \quad r \to \infty. \tag{3.1d}$$

In this section (3.1) is considered in the limit $H \to \infty$ with Re constant. This corresponds to considering progressively deeper flows while holding constant the obstacle shape,

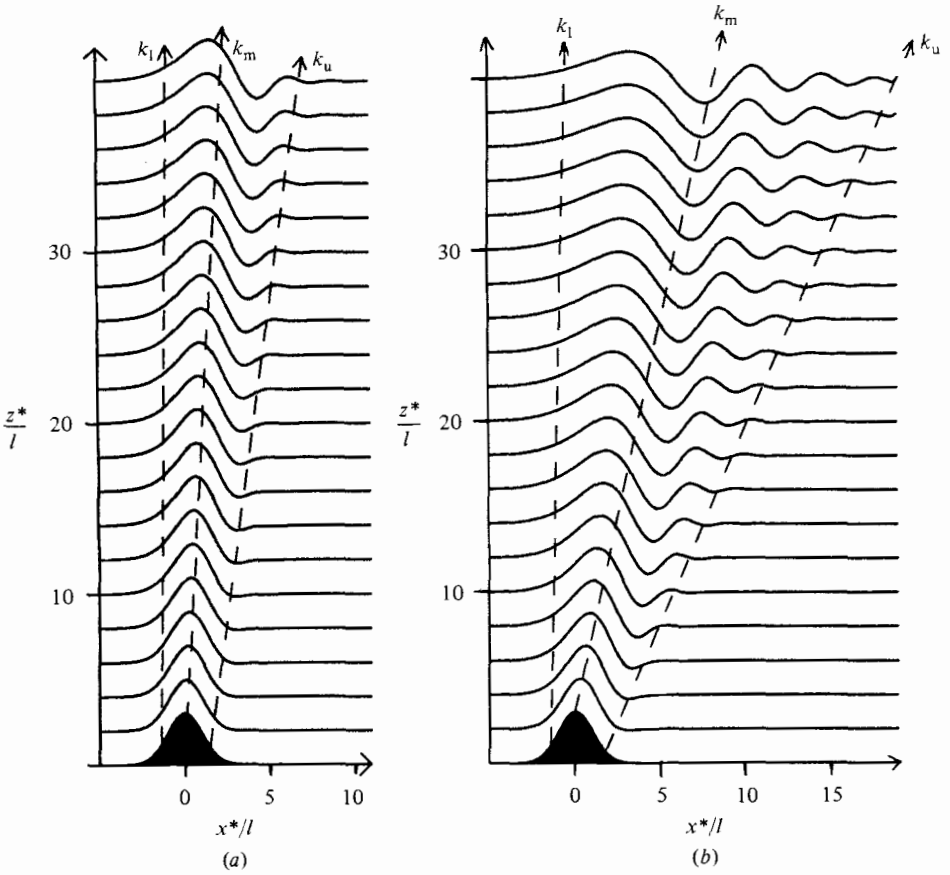

FIGURE 1 (*a*, *b*). For caption see p. 366.

rotation rate, viscosity and upstream velocity. Since the obstacle acts as a localized source of inertial waves which disperse along straight paths, the amplitude of the motion decays inversely as the square root of the height even for inviscid motion (e.g. Whitham 1974). Thus for $H^{\frac{1}{2}} \gg 1$ the amplitude of the motion at the upper boundary is small, the effects of vortex compression and inertial wave reflections, negligible, and the boundary condition (3.1*c*) may be replaced by the requirement that w does not grow exponentially with Z.

Introducing Fourier transforms in the form

$$\hat{f}(k) = \int_{-\infty}^{\infty} f(x)\ e^{-ikx}\,dk \tag{3.2}$$

gives

$$\frac{d^2\hat{w}}{dZ^2} = -k^4(1 - iRe^{-1}k)^2\hat{w}. \tag{3.3}$$

Thus $\hat{w} = W_0(k)\exp\{-(i + Re^{-1}k)|k|Z\}$, where the choice of sign in the exponent is determined by the boundedness condition for large Z, and W_0 is evaluated from the boundary conditions. This gives

$$w = \frac{\alpha}{2\pi}\int_{-\infty}^{\infty} \frac{ik\hat{f}(k)}{1 + E^{\frac{1}{2}}|k|} \exp\{-k^2|k|Re^{-1}Z - ik|k|Z + ikx\}\,dk \tag{3.4a}$$

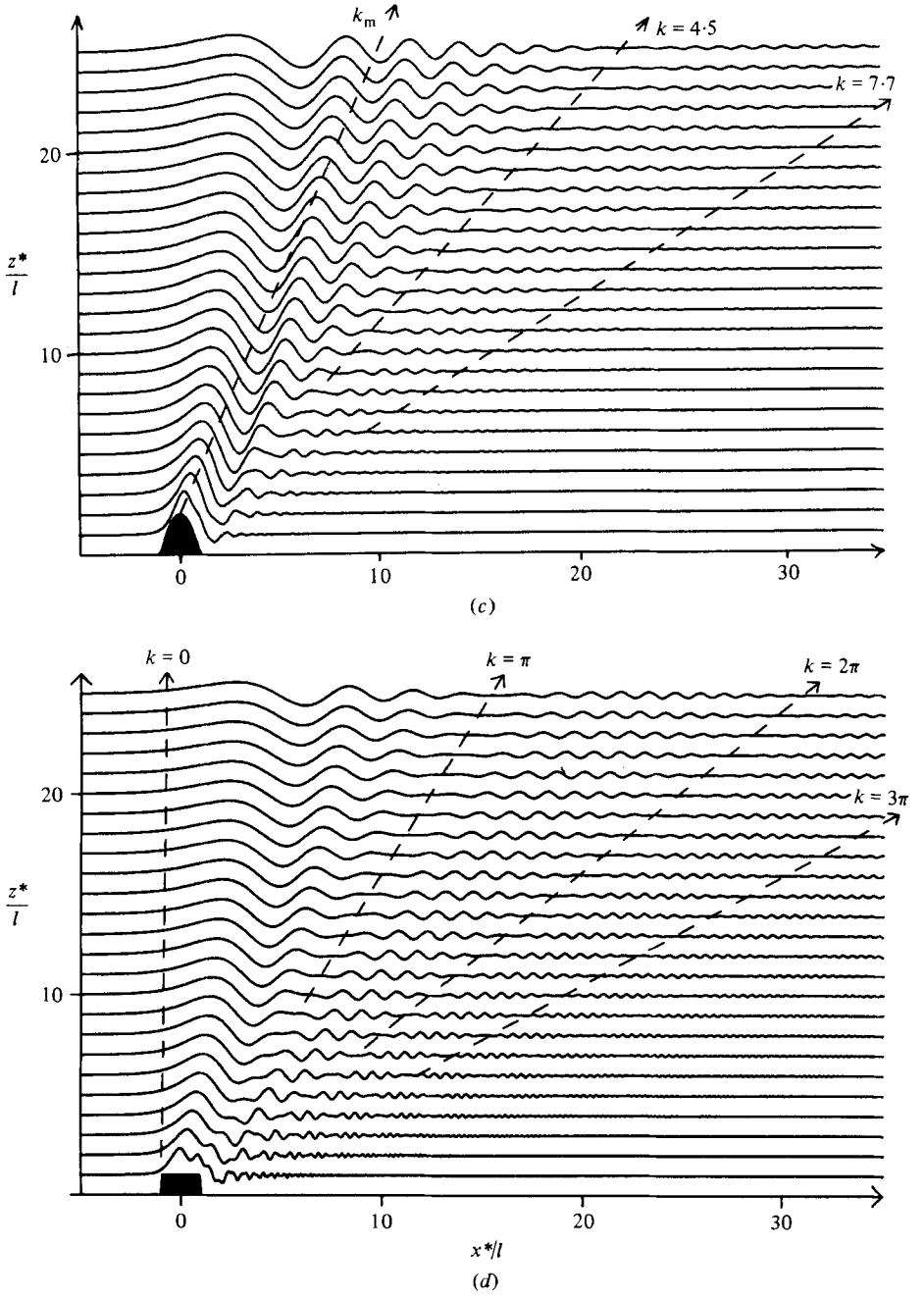

FIGURE 1. Infinitely deep inviscid ($E = 10^{-6}$) flow over: (*a*) the Gaussian ridge f_1 with $Ro = 0{\cdot}033$, $\alpha = 3$; (*b*) f_1 with $Ro = 0{\cdot}1$, $\alpha = 3$; (*c*) the parabolic ridge f_2 with $Ro = 0{\cdot}1$, $\alpha = 2$; (*d*) the top-hat ridge f_3 with $Ro = 0{\cdot}1$, $\alpha = 1$.

$$= \frac{\alpha}{\pi}\int_0^\infty \frac{k\hat{f}(k)}{1+E^{\frac{1}{2}}k}\exp\{-k^3Re^{-1}Z\}\sin(k^2Z-kx)\,dk \tag{3.4b}$$

when f is even. The corresponding result for ζ is

$$\zeta = \frac{\alpha}{\pi}\int_0^\infty \frac{\hat{f}(k)}{1+E^{\frac{1}{2}}k}\exp\{-k^3Ez_\infty^*/l\}\cos(k^2z_\infty^*\,Ro/l-kx)\,dk. \tag{3.5}$$

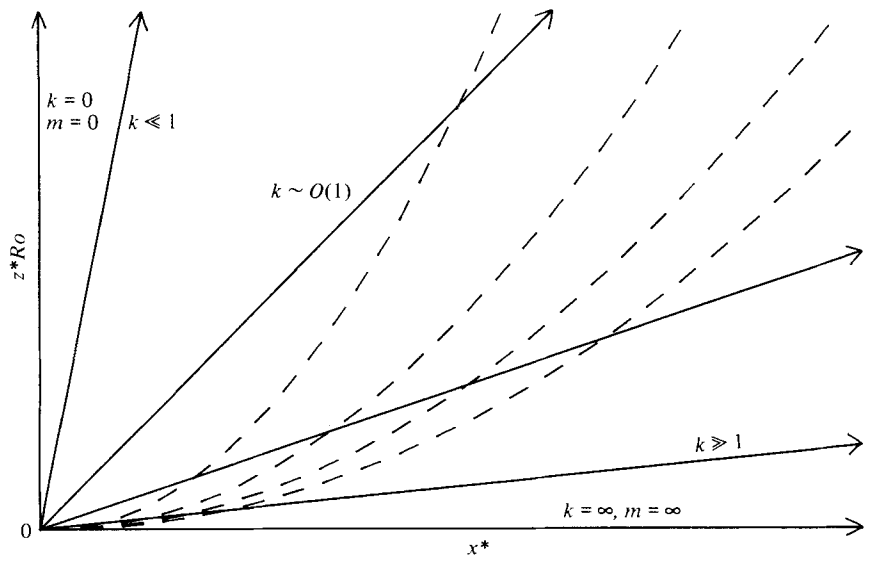

FIGURE 2. Ray paths (——) and phase lines (— — — —) for the problem (after Whitham 1974).

This integral may be evaluated numerically using well-known efficient routines for the inversion of Fourier transforms. Figure 1 gives particle paths for effectively inviscid flow ($E = 10^{-6}$). The paths in figures 1 (a, b) are for the obstacle $f_1(x) = \exp(-\frac{1}{2}x^2)$, for which $\hat{f}_1 = (2\pi)^{\frac{1}{2}} e^{-\frac{1}{2}k^2}$. The paths in figure 1 (c) are for $f_2(x) = 1 - x^2$ if $|x| < 1$, $f_2(x) = 0$ if $|x| > 1$, for which $\hat{f}_2 = 4([\sin k]/k - \cos k)/k^2$, and figure 1 ($d$) is for $f_3(x) = 1$ if $|x| < 1$, $f_3(x) = 0$, $|x| > 1$, for which $\hat{f}_3 = 2(\sin k)/k$.

A description of the observed flow patterns may be obtained by considering wavelike solutions of (2.7) following Lighthill (1967). Substituting the form

$$\exp(-i\omega t + ikx + im\bar{z}),$$

where $\bar{z} = z^*/l$, gives the dispersion relation,

$$\omega = k \pm m/kRo - iRe^{-1}k^2. \tag{3.6}$$

This corresponds to a wave of frequency $k \pm m/kRo$, which decays at a rate $Re^{-1}k^2$ per unit time as it propagates through the medium. The group velocity corresponding to the inviscid ($Re = \infty$) form of (3.6) is

$$\mathbf{c}_g = (1 \mp m/k^2Ro, \pm 1/kRo). \tag{3.7}$$

Discarding incoming waves from infinity, which have $\partial\omega/\partial m < 0$, gives the steady inviscid solution of (3.6): $m = -k|k|Ro$, with $\mathbf{c}_g = (2, 1/|k|Ro)$. This is closely related to the problem of flexural vibrations in a beam (Whitham 1974). Waves propagate energy upwards and behind obstacles along straight rays $x^* = 2|k|z^*Ro$, with *long* waves travelling fastest. The important wavenumbers at a point $(x, \bar{z})$ are thus $k = \pm x/2\bar{z}Ro$, giving a phase $\pm x^2/4\bar{z}Ro$, constant on parabolas, and an attenuation factor $\exp(-Ex^3/8\bar{z}^2Ro^3)$. The ray paths and phase lines for this problem are given in figure 2.

Lighthill (1967 and HIL) and Whitham (1974) point out that the region of maximum perturbation away from a wave source in a dispersive medium is determined by the

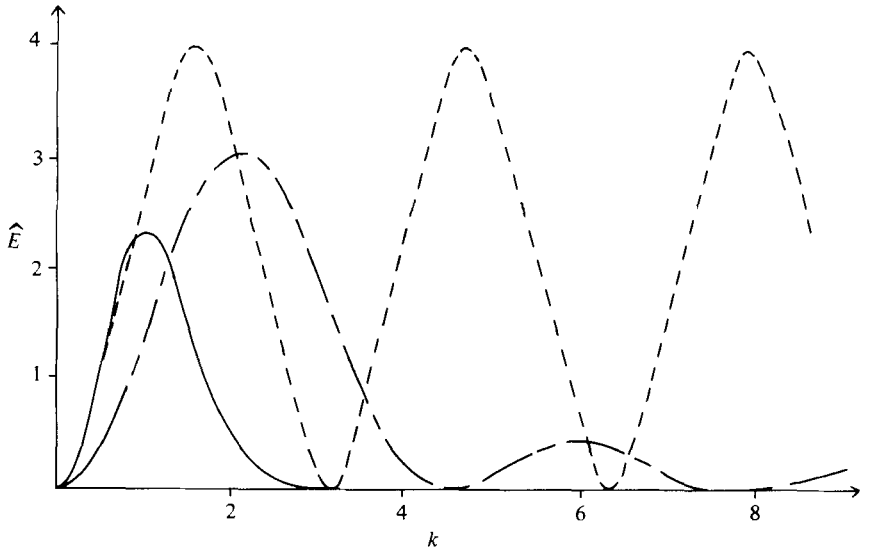

FIGURE 3. The energy spectra of the disturbance excited by the obstacle: ——, the Gaussian ridge f_1; – — –, the parabolic ridge f_2; – – – –, the top-hat ridge f_3.

wavenumber spectrum excited by the source. The importance, in the present problem, of a given wavenumber may be estimated from the known vertical kinetic energy associated with the wavenumber on the lower boundary

$$\hat{E}(k) = |\hat{w}(k)|_{z=0}|^2 = k^2\hat{f}^2. \tag{3.8}$$

The energy spectra for the obstacles f_1, f_2 and f_3 are given in figure 3. For the obstacle f_1, $\hat{E}_1(k) = 2\pi k^2 e^{-k^2}$, with maximum at $k_m = 1$ and 95 % of the energy lying between the wavenumbers $k_l = 0{\cdot}26$ and $k_u = 2{\cdot}05$. Hence the disturbance has dominant wavenumber unity, and is confined to the beam

$$2k_l Ro \leqslant x^*/z^* \leqslant 2k_u Ro. \tag{3.9}$$

The upstream limit of energy propagation is thus given by a line of slope $2k_l Ro$ starting from the upstream edge of the obstacle and the downstream limit by a line of slope $2k_u Ro$ from the downstream edge. These lines are shown dashed in figure 1, and may be seen to contain the majority of the flow perturbation. The maximum disturbance within this region occurs on the ray of slope $2k_m Ro$ originating at the top of the ridge. The phase of this disturbance at a given height is $k_m^2 \bar{z} Ro = \bar{z} Ro$, varying on a length scale of l/Ro. Thus the maximum disturbance cannot be associated with a positive 'columnar' displacement for $\bar{z} Ro > \frac{1}{2}\pi$. In fact for $\bar{z} Ro \simeq \pi$, the maximum displacement is associated with a trough. Within the region (3.9), a disturbance has constant phase on a parabola and attains its maximum amplitude where that parabola intersects the ray $x^* = 2k_m Roz^*$.

For the obstacle f_2 the wavenumber associated with maximum energy is $k_m \simeq 2{\cdot}1$ and bounds on the energetic wavenumbers are approximately $k_l = 0{\cdot}5$ and $k_u = 4$. The disturbance energy occupies a wavenumber range ($k_u - k_l \simeq 3{\cdot}5$), double that of f_1, and so, by a given height, disperses over a region of twice the horizontal extent. The amplitude of the disturbance (proportional to the square root of the energy density) thus decays approximately 50 % more rapidly than for f_1. Since k_m for f_2 is

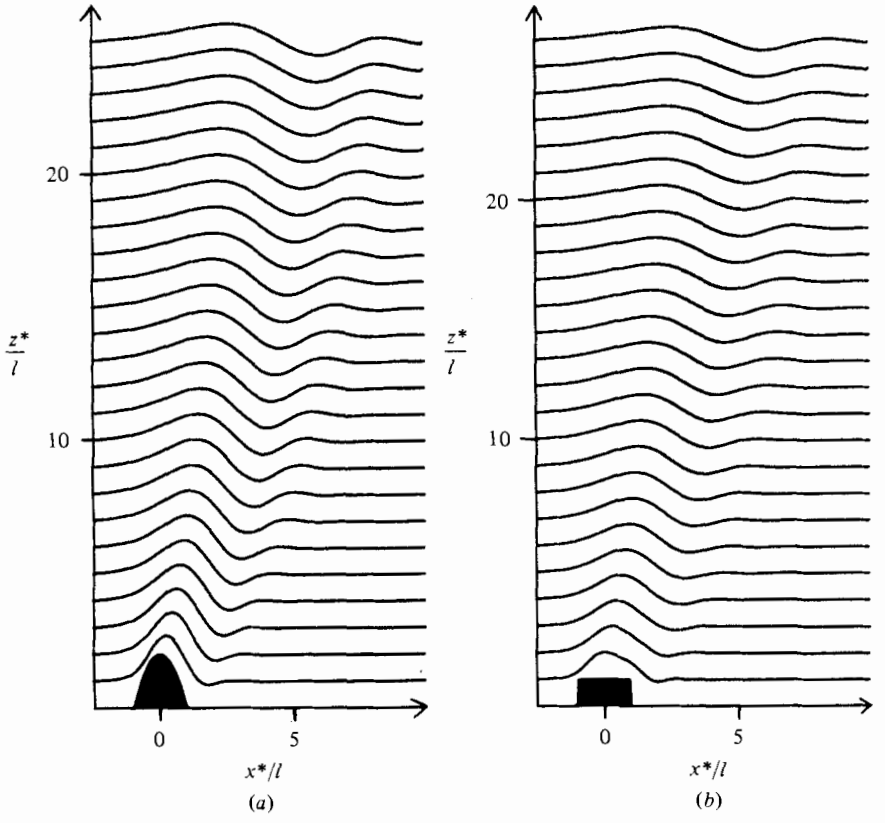

FIGURE 4. Particle paths for infinitely deep viscous ($E = 10^{-2}$) flow at $Ro = 0{\cdot}1$ over (*a*) the parabolic ridge f_2 ($\alpha = 2$) and (*b*) the top-hat ridge f_3 ($\alpha = 1$).

double k_m for f_1, the phase change of the maximum disturbance with height is twice as rapid as for f_1. From figure 3, it may be noted that $\hat{E}_2$ vanishes at $k \simeq 4{\cdot}5$ and $k \simeq 7{\cdot}7$. These rays are marked on figure 1 (*c*), and can be seen to be directions of zero perturbation, as would be expected.

The obstacle f_3 does not satisfy the implicit assumption in the model that topographic slopes are of order unity, and this is reflected in the fact that the energy associated with the disturbance is infinite. Nevertheless, retaining the highest-order horizontal derivatives, (3.5) resolves thin vertical shear layers present at discontinuities in topographic slope to give solutions that should represent close approximations to flow of a real fluid over discontinuous topography. As with f_2, there are an infinite number of directions of zero perturbation; given here by $k = n\pi$, $n = 0, 1, 2, \ldots$. Between these directions are regions of flow perturbation of equal energy. For this obstacle shape, the whole region behind the obstacle is filled with lee waves.

Viscosity introduces damping proportional to the cube of the horizontal wavenumber. Thus flow perturbations corresponding to moderate or large k, which (see figure 2) occur along rays with slopes of order Ro^{-1} or less, are strongly attenuated and there is little disturbance in the downstream wedge $0 < z^*/x^* < O(Ro^{-1})$. Viscosity causes the dominant disturbance to decay at a rate $Re^{-1}k_m^2$ per unit time. This corresponds to a decay of Ek_m^3 per unit height or $\frac{1}{2}Re^{-1}k_m^2$ per unit distance horizontally,

and so introduces an e-folding height $z_e = E^{-1}k_m^{-3}l$ and an horizontal e-folding length $x_e = 2Rek_m^{-2}l$.

Flow over the obstacle f_1, which has little energy at high wavenumber and for which $z_e \simeq l/E$ is large compared with flow depths, is almost unaffected by values of E of order 10^{-2} or smaller. Figure 4(a) gives particle paths for the obstacle f_2 and for $E \simeq 10^{-2}$. The high-wavenumber disturbance previously present in the region $x^* > 4Roz^*$ is now absent, and the disturbance decays with scales $(x_e, z_e) = (5l, 12l)$. Figure 4(b) shows the paths over the obstacle f_3 for the same value of E. Once again, all high-wavenumber perturbations are removed, and the flow is quiescent in the region $x^* > \pi Roz^*$. The perturbation also decays rapidly with height, the particle paths having the same general behaviour as those given for flow over an upright circular cylinder in HIL. For both these flows, the inclusion of a solid boundary at $z^* = O(20l)$ would have little effect on the flow field.

Whether a disturbance is attenuated by the upper boundary depends strongly on obstacle shape. A tank of depth h will be effectively infinite only if

$$[(k_u - k_l)hRo/l]^{-\frac{1}{2}} \exp(-k_m^3 Eh/l) \ll 1. \tag{3.10}$$

The first factor in (3.10) gives the algebraic decay due to dispersion, and the second gives the exponential decay due to internal dissipation. Flows for which this factor is not necessarily small are considered in §4.

Some of the above results may also be obtained by a steepest-descent estimate of (3.4) for Z large, with $x/Z \sim 1$. Then

$$w = \frac{\alpha}{\pi}\mathscr{I}\int_0^\infty \frac{\hat{f}(k)}{1+E^{\frac{1}{2}}k}\exp[ZF(k)]\,dk \tag{3.11}$$

$$\sim (\pi Z)^{-\frac{1}{2}}(1+(3x/ReZ)^2)^{\frac{1}{8}}\mathscr{I}\left\{\frac{k_0\hat{f}(k_0)}{1+E^{\frac{1}{2}}k_0}\exp\left[ZF(k_0)+\tfrac{1}{4}i\pi+i\operatorname{Arctan}\frac{3x}{4ReZ}\right]\right\}, \tag{3.12a}$$

where

$$F(k) = -Re^{-1}k^3 - ik^2 + ikx/Z, \quad k_0 = [1-(1+3ix/ZRe)^{\frac{1}{2}}]Re/3i.$$

For $Ex/Ro^2\bar{z} \ll 1$, the leading-order terms give $k_0 = x/2Ro\bar{z}$ and

$$\exp\left\{\frac{E}{8R_0^3}\frac{x^3}{\bar{z}^2}\right\}w \sim \frac{\hat{f}(x/2Ro\bar{z})}{E^{\frac{1}{2}}+2\bar{z}Ro/x}[\pi\bar{z}Ro]^{-\frac{1}{2}}\sin\left[\frac{x^2}{4\bar{z}Ro}-\frac{3Ex}{8R_0^2\bar{z}}-\tfrac{1}{4}\pi\right]+O((\bar{z}Ro)^{-1}). \tag{3.12b}$$

Expression (3.12b) shows that Ekman pumping introduces an algebraic (to $O(Ro)$) downstream decay with scale $E^{-\frac{1}{2}}$ and that internal dissipation displaces the parabolas of constant phase. The first maximum of displacement occurs at the first zero of w, which is given by

$$\pi\bar{z}Ro = x(x - \tfrac{3}{2}Re^{-1}).$$

For Reynolds numbers of order unity, lines of constant phase contain a term linear in x as well as the inviscid term quadratic in x. Hence constant-phase lines are straighter in viscous flow near topography than in the corresponding inviscid flow.

At any point in the flow, the amplitude of the disturbance decreases with increasing viscosity. However, at a fixed downstream station the magnitude of this decrease itself decreases with increasing height. In fact, as $\bar{z}\to\infty$ for x fixed, (3.12b) gives $\zeta \sim (\pi\bar{z}Ro)^{-\frac{1}{2}}\mathscr{A}$, independently of Re, where $\mathscr{A} = \hat{f}(0)$ is the cross-sectional area of the

ridge. Since the region $\bar{z}/x \gg Ro$ is occupied by the longest waves, the eventual decay of the disturbance with height (at fixed x) is due to dispersion and is independent of viscosity. However, for a wave spectrum with a well-defined dominant wavenumber the station corresponding to the dominant disturbance moves downstream with increasing height, giving the decay on scales x_e and z_e noted previously.

The variation with downstream displacement of the wake at a given height may be obtained by considering the asymptotic limit of (3.11) given by $x \gg 1$, $x/Z \sim 1$. This gives precisely the result (3.12*b*) with the term $(\pi \bar{z} Ro)^{-\frac{1}{2}}$ replaced by $(\pi x)^{-\frac{1}{2}}$ and an error term $O(x^{-1})$. Hence the downstream attenuation of the wake is given by

$$x^{-\frac{1}{2}}(1+E^{\frac{1}{2}}x/2\bar{z}Ro)^{-1}\exp(-Ex^3/8\bar{z}^2Ro^3)\hat{f}(x/2\bar{z}Ro).$$

At a given height, the wake decays exponentially in a viscous flow, and in inviscid flow at a rate determined by the rate of decay with increasing wavenumber of the excited inertial wave spectrum. Thus the wake decays exponentially for f_1, as $x^{-\frac{5}{2}}$ for f_2, and as $x^{-\frac{3}{2}}$ for f_3. This result may also be derived from formulae in SC in the limit $H \to \infty$, but disagrees with the result of Cheng (1977) that the wake behind a three-dimensional isolated obstacle does not decay downstream. A revised version of Cheng's (1977) analysis in Cheng & Johnson (1982) obtains the downstream decay.

In the analysis and examples presented above, Ekman pumping, which introduces downstream decay on a scale of order $E^{-\frac{1}{2}} = (Re/Ro)^{\frac{1}{2}} \sim O(Ro^{-\frac{1}{2}})$ is of secondary importance to internal dissipation with a decay scale of $Re \sim O(1)$. This corresponds to experimental observations of more viscous flow but not to typical geophysical flows. In flows where $Re \sim O(Ro^{-1})$, i.e. $E \sim Ro^2$, the two mechanisms are of comparable strength, introducing decay on a scale of order Ro^{-1}, and when $Re \gg Ro^{-1}$, i.e. $E \ll Ro^2$, Ekman pumping dominates. However, viscosity is then no longer a zeroth-order effect, and to lowest order the motion is undamped. Low-Rossby-number geophysical flows are also characterized by values of H that are of order unity or less, and it is shown in §4 that for H sufficiently small (although h/l may still be large) viscous attenuation can be a zeroth-order effect even when $Re \gg Ro^{-1}$.

4. Finite-depth container

In this section the structure of the standing inertial lee-wave wake present for finite H for sufficiently small E is considered. The solution of (2.10) may be obtained by introducing the Fourier transform (3.2) and solving the resulting linear ordinary differential equation in z_∞. This gives

$$\zeta = \frac{\alpha}{2\pi}\int_{-\infty}^{\infty} \hat{f}(k)\cos\theta \frac{\sin[Hm(1-z_\infty)-\theta]}{\sin[Hm-2\theta]} e^{ikx}\,dk, \tag{4.1}$$

where $\theta = \mathrm{Arctan}(iE^{\frac{1}{2}}k)$ and $m = k^2 - iRe^{-1}k^3$, which reduces to (3.5) in the limit $H \to \infty$. The integral may be evaluated straightforwardly for the obstacle f_2 by writing

$$\hat{f}_2 = 2k^{-3}\{(i-k)e^{-ik} - (i+k)e^{ik}\}. \tag{4.2}$$

Then

$$\zeta = \alpha\{G_1(x+1, z_\infty) - G_2(x-1, z_\infty)\}, \tag{4.3a}$$

where

$$G_{1,2}(x,z) = \frac{1}{\pi}\int_{-i\infty}^{i\infty} \frac{1 \mp s}{s^3} \frac{\sin[Hm(1-z)-\theta]}{\sin[Hm-2\theta]} \cos\theta\, e^{sx}\,ds, \tag{4.3b}$$

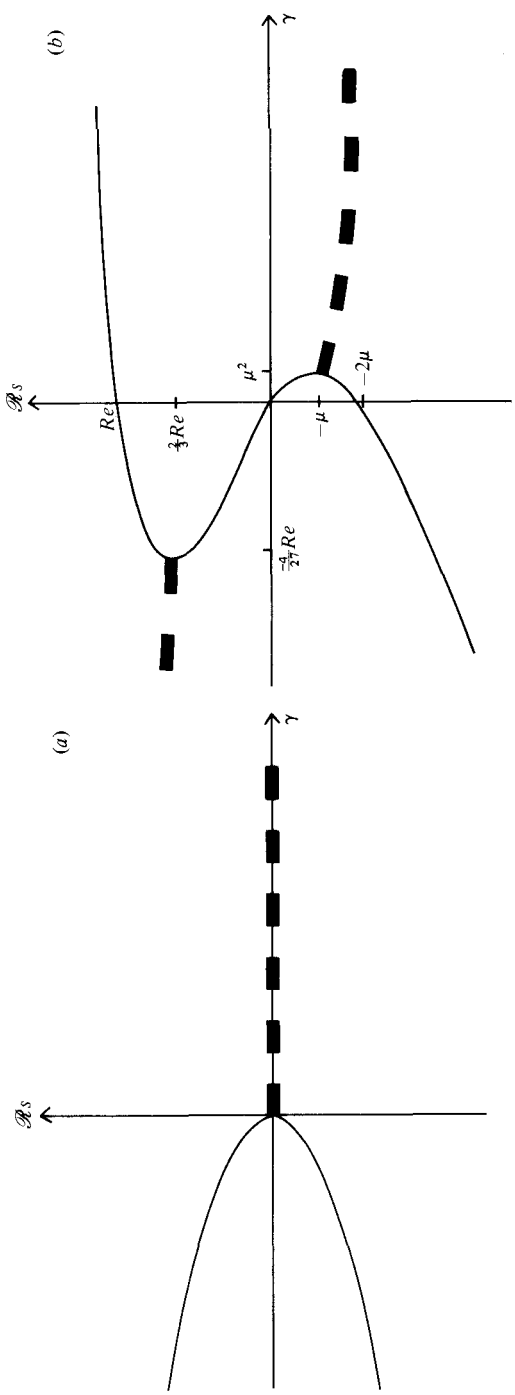

FIGURE 5. (*a*) Roots of the inviscid equation $-s^2 = \gamma$. The solid lines are real roots, the dashed lines the real part of a complex-conjugate pair. (*b*) As in (*a*) but for the viscous equation $Re^{-1}s^3 - s^2 - 2\mu s = \gamma$.

the upper sign giving G_1 and the lower G_2. The path of integration is along the imaginary s-axis and $m = Re^{-1}s^3 - s^2$, with $\theta = \text{Arctan}\,(E^{\frac{1}{2}}s)$, $|\theta| < \frac{1}{2}\pi$ for s real. For $x > 0$, $G_{1,2}(x, z)$ are given by the sum of residues in the half-plane $\mathscr{R}s < 0$. Upstream ($x < 0$), the residues in $\mathscr{R}s > 0$ sum to $-G_{1,2}(x, z)$. The poles of the integrand occur when

$$Re^{-1}s^3 - s^2 - \frac{2}{H}\,\text{Arctan}\,(E^{\frac{1}{2}}s) = \frac{n\pi}{H} \quad (n = 0, \pm 1, \pm 2, \ldots). \tag{4.4}$$

Replacing the inverse tangent by the first term of its Taylor series gives a cubic whose roots are close approximations to those of (4.4), namely

$$Re^{-1}s^3 - s^2 - 2\mu s = n\pi/H \quad (n = 0, \pm 1, \pm 2, \ldots). \tag{4.5}$$

The discussion of the inversion of (4.3) will be based on (4.5) with Re^{-1}, μ small, although the numerical illustrations will be obtained using (4.4). Figure 5 gives the graphs of the roots of (4.5); the solid lines representing real roots, the dashed lines the real part of complex-conjugate pairs. Figure 5(a) is for the inviscid case $E = 0$ and figure 5(b) for the viscous case. The complex-conjugate roots in figure 5(a) have real part zero, and so may be included in either the upstream or downstream solution. By considering an initial-value problem SC showed that these non-decaying waves occur downstream of an obstacle. The inclusion of viscosity also removes the ambiguity of the inviscid steady problem for all but the $s = 0$ contribution. For this pole the initial-value analysis shows its contribution occurs in $x > 0$.

For each n in (4.4) there are three contributions to $G_{1,2}$. These contributions differ in three ranges of n.

(i) $n\pi/H \gtrsim \mu^2$. Equation (4.5) has one positive root and a complex-conjugate pair of roots with negative real parts. The real root, at $s > Re$, is a vertical shear-layer contribution, making a negligible contribution to $G_{1,2}$ outside regions of thickness $O(Re^{-1})$ of discontinuities in topography. The complex-conjugate pair, for $n < 6\pi H/\mu^2$, satisfy

$$-\mu - n\pi/2HRe \leqslant \mathscr{R}s < -\mu - n\pi/12HRe, \tag{4.6a}$$

$$\tfrac{1}{6}(n\pi/H)^{\frac{1}{2}} < |\mathscr{I}s| \leqslant (n\pi/H)^{\frac{1}{2}}, \tag{4.6b}$$

with equality holding when $E = 0$. Thus the wavelength of the downstream wake is unaltered to lowest order, but the amplitude is no longer constant in x, decaying exponentially owing to the combined effects of Ekman pumping and internal dissipation. These are the decay rates given by SC in their discussion of viscous effects. The Ekman-pumping attenuation is independent of mode number n, representing a decay of the whole disturbance on the standard Ekman-pumping scale of $\mu^{-1}l = E_{\mathrm{v}}^{-\frac{1}{2}}l/Ro$. The effect of internal dissipation increases with increasing mode number. In a flow with H small only a few wavelengths of the lowest-order lee-wave modes will be present – the number of wavelengths and modes decreasing as $H \to 0$.

(ii) $-\frac{4}{27}Re^2 < n\pi/H < \mu^2$. The roots of (4.5) are real, corresponding to monotonically decaying solutions. When $n = 0$ the dominant contributions come from poles at $s = 0$ and $s \simeq -2\mu$, giving a columnar disturbance and the downstream Ekman pumping caused by the vorticity associated with the column.

(iii) $n\pi/H < -\frac{4}{27}Re^2$. There is one negative real root of (4.5) giving a monotonically decaying downstream contribution and a complex-conjugate pair. This pair gives an order-one contribution within vertical shear layers but is negligible outside regions of thickness $O(Re^{-1})$ of discontinuities in topography.

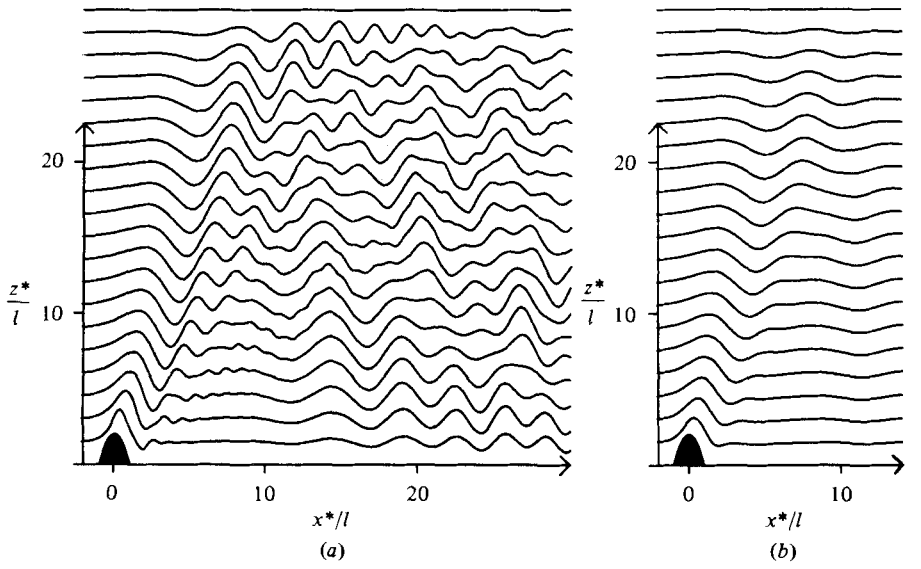

FIGURE 6. Finite depth ($h/l = 30$, $\alpha = 2$) flow over the parabolic ridge f_2 at $Ro = 0{\cdot}1$: (*a*) inviscid ($E = 10^{-6}$); (*b*) viscous ($E = 10^{-2}$).

With two exceptions, the poles of the integrand are simple. If $n\pi/H$ coincides with one of the turning points of (4.4) then two poles coalesce. The presence of this second-order pole does not affect the behaviour of the solution, and so is neglected. The pole at $s = 0$ is third-order owing to the form (4.2) of $\hat{f}_2$. This pole contributes that part of the solution which satisfies the inhomogeneous boundary condition. For the obstacle f_3, for which $\hat{f}_3 = ik^{-1}(e^{-ik} - e^{ik})$, this pole would be of order one. Denoting the three roots of (4.4), for given n, by $\omega_{n,i}$ ($i = 1, 2, 3$) and the Heaviside unit function by $\mathscr{H}$ (with $\mathscr{H}(x)$ unity if $x > 0$, zero if $x \leqslant 0$), gives

$$G_{1,2}(x,z) = -\tfrac{1}{2}x^2 \pm x + (z - \tfrac{1}{2})(x \mp 1 - \tfrac{1}{2}HE^{-\frac{1}{2}} - Re^{-1})HE^{-\frac{1}{2}} + \sum_{n=-\infty}^{\infty}\sum_{i=1}^{3} \mathscr{R}\mathscr{F}(x,z,\omega_{n,i})\mathscr{H}(-\mathscr{R}\omega_{n,i}) \quad (x > 0), \tag{4.7a}$$

$$G_{1,2}(x,z) = -\sum_{n=-\infty}^{\infty}\sum_{i=1}^{3} \mathscr{R}\mathscr{F}(x,z,\omega_{n,i})\mathscr{H}(\mathscr{R}\omega_{n,i}) \quad (x < 0), \tag{4.7b}$$

where

$$\mathscr{F}(x,z,s) = \frac{-(1 \mp s)(1 + Es^2)^{\frac{1}{2}} \sin[n\pi z + (2z-1)\operatorname{Arctan}(E^{\frac{1}{2}}s)]}{s^3\{(1 + Es^2)(1 - \frac{3}{2}s/Re)Hs + E^{\frac{1}{2}}\}} e^{sx}. \tag{4.8}$$

The solution consists of an infinite number of sinusoidal vertical modes, phase-shifted owing to Ekman pumping, and reduces in the limit $E \to 0$ to that given in SC (modified for the present obstacle shape). The amplitude of each mode is proportional, for large Re, to $H^{-\frac{1}{2}}\hat{f}((n\pi/H)^{\frac{1}{2}})$. For $H \gg 1$ all modes for which n is of order H/π or smaller contribute to the solution. The dominant contributions in $x < H$ correspond to points of stationary phase in the integral (3.3) and, since n is of order H, the wake decays downstream on a scale of order $l/(Re^{-1} + \mu) \simeq lRe$ (from 4.6*a*). For $H \ll 1$ the amplitude of a given mode is determined by the behaviour of $\hat{f}$ for large values of its argument: the smoother the topography the fewer modes required to model the flow. Since n is

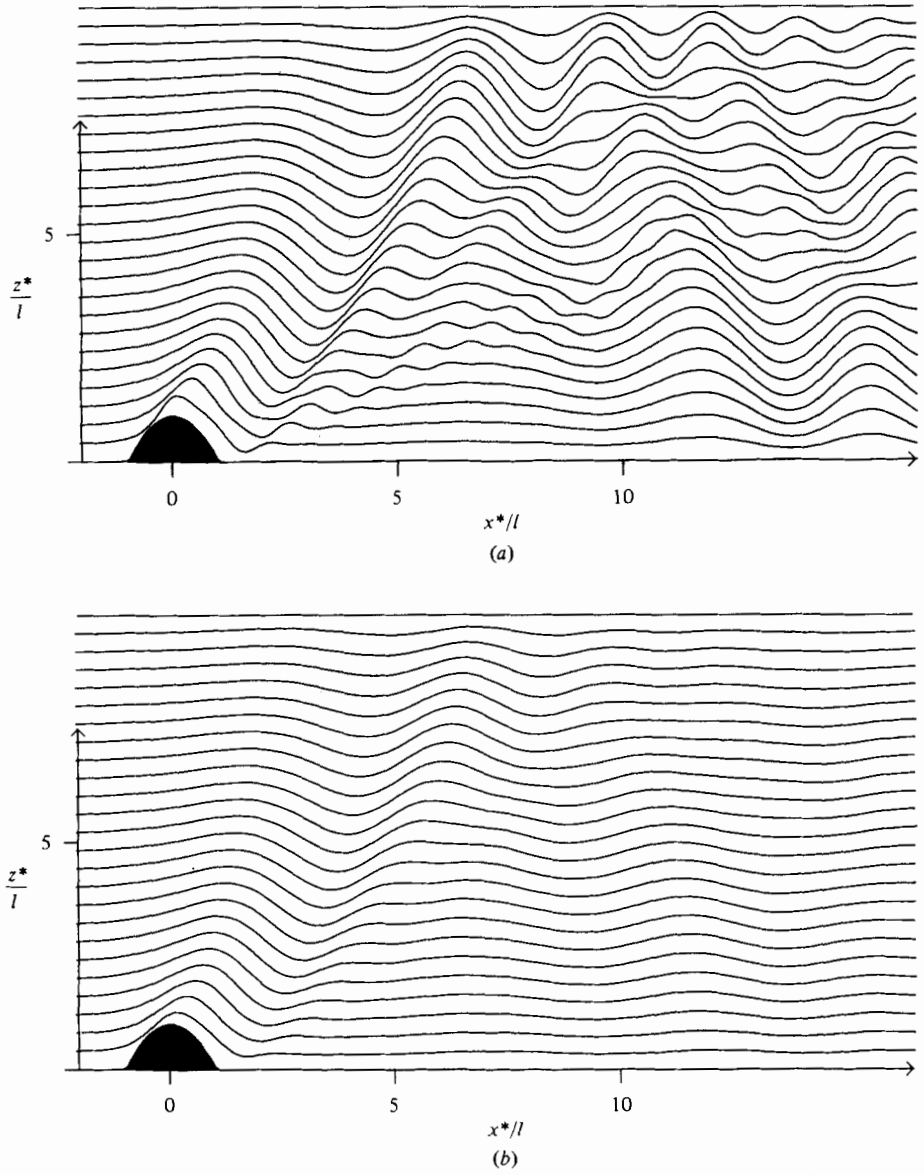

FIGURE 7. Finite-depth ($h/l = 10$, $\alpha = 1$) flow over the parabolic ridge f_2 at $Ro = 0{\cdot}2$: (*a*) inviscid ($E = 10^{-6}$); (*b*) viscous ($E = 10^{-2}$).

of order unity the decay scale of the wake is more rapid. From (4.6*a*), the wake decays on a length scale of order

$$Hl/\{Re^{-1} + E^{\frac{1}{2}}\}. \tag{4.9}$$

Figure 6 gives particle paths for $H = 3$ and $Ro = 0{\cdot}1$. The paths in figure 6(*a*) for the inviscid case ($E = 10^{-6}$) show the wave packet spreading behind the obstacle with the phase of the maximum disturbance changing by $k_m^2 H = 4\pi$ by the upper boundary. Thus for $z^* > \frac{1}{4}h$ the maximum disturbance can no longer be associated with a leaning column. For $z^* < \frac{1}{4}h$, directly above the obstacle, the contributions from the lower-order modes $n = \pm 1, \pm 2, \ldots$ are equal and opposite, and cancel the zeroth-order mode

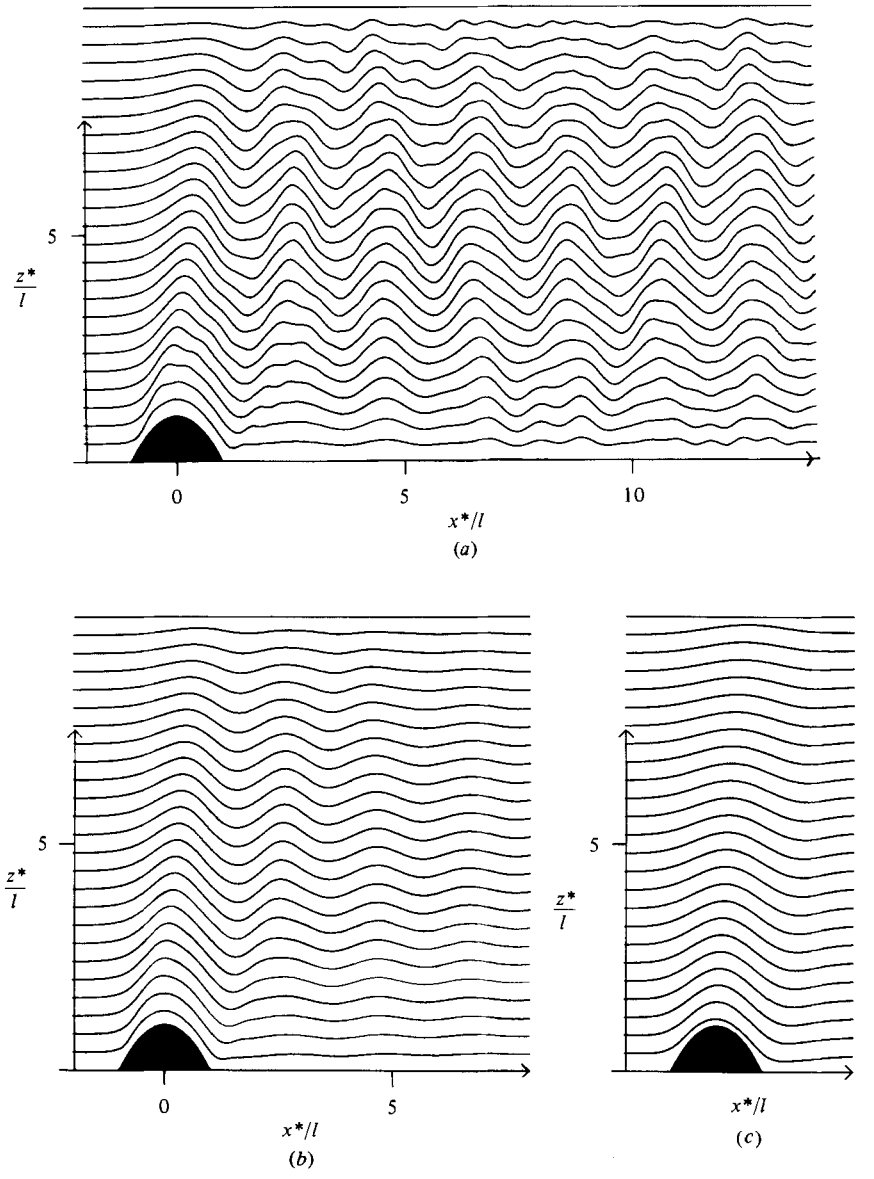

FIGURE 8. Finite-depth ($h/l = 10$, $\alpha = 1$) flow over the parabolic ridge f_2 at $Ro = 0{\cdot}033$: (*a*) inviscid ($E = 10^{-6}$); (*b*) $E = 10^{-3}$; (*c*) viscous ($E = 10^{-2}$).

columnar contribution to give little disturbance as in points of non-stationary phase in the case of infinite depth. The wave packet is reflected from the upper boundary, returning to the lower boundary by $x = 4k_m H \simeq 24$ and so leaving a quiescent region behind the obstacle. It is within this region, $0 \lesssim \bar{z} \lesssim O(Ro^{-1})$ and $x \lesssim O(4k_m H)$ that the flow appears to be a leaning columnar disturbance; a locally important horizontal wavenumber may be defined and the flow described simply in terms of ray paths. For $x > O(4k_m H)$ the multiplicity of ray paths through each point means that there is no single locally important wavenumber and no simple description in terms of ray paths. The disturbance forms the curtain of an inertial wave wake described in SC. No wave

energy escapes from the downstream region, so the inviscid wake is unattenuated.† The downstream amplitude of the wake may be estimated by noting, from § 3, that the strength of the wake is independent of H for $H \gg 1$. Thus the energy transported past any fixed station $x = x_0 \gg H$ is independent of H for $H \gg 1$. Hence the energy density is inversely proportional to H, and so the amplitude of the wake is proportional to $H^{-\frac{1}{2}}$. The wake is insensitive to obstacle shape in this region. For the viscous case (figure 6*b*), where $E = 10^{-2}$ and the infinite-depth decay scales are $(x_e, z_e) = (5l, 12l)$, the maximum disturbance decays before its change of phase becomes apparent, i.e. at $z^* = \frac{1}{4}h$.

Figure 7(*a*) gives paths for $H = 2$, $Ro = 0{\cdot}2$, $E = 10^{-6}$. The cancellation of the lower-order modes near $x = 0$ for $z^* > \frac{1}{3}h$ (i.e. a phase change of π in the maximum disturbance) is more pronounced than in figure 6(*a*). The majority of the upward perturbation occurs in the parabola of constant phase originating behind the obstacle. Once again a quiescent region of height $O(Ro^{-1})$ and length $O(4k_m H) \simeq 16$ is present behind the obstacle. The viscous case (figure 7*b*) ($E = 10^{-2}$), with $(x_e, z_e) \simeq (10l, 12l)$ shows the disturbance decaying by the upper boundary since $k_m^3 Eh/l \sim 1$.

Figure 8 gives paths for the same geometry with $Ro = 0{\cdot}033$, so $H = \frac{1}{3}$. Since the maximum disturbance changes phase by only $k_m^2 H \simeq \frac{1}{3}$ by the upper boundary, it may be identified over the whole fluid depth with a leaning columnar disturbance. This is not the sole feature of an inviscid flow. Figure 8(*a*) ($E = 10^{-6}$) shows that the quiescent region is absent (since $4k_m H$ is of the order of the obstacle width). There is no single locally important horizontal wavenumber downstream from the obstacle, and the inertial-wave curtain occurs immediately. However, because H is small, only the lowest vertical modes contribute, the wake containing predominantly mode one and extending downstream with undiminishing amplitude. Since only the lowest modes are present, the appropriate viscous decay scale is given by (4.9). In figure 8(*b*) ($E = 10^{-3}$) attenuation due to Ekman pumping (with scale $lHE^{-\frac{1}{2}} \sim 10l$) is of equal importance to that due to internal dissipation (with scale $HRe \sim 10l$), giving a combined decay scale of order $5l$. In the more viscous flow (figure 8*c*) ($E = 10^{-2}$) internal dissipation (with scale l) once again dominates Ekman pumping (with scale $3l$) and the wake decays within one obstacle width.

The enhanced dissipation in shallower flows evident in figure 8 is manifested to a greater degree in figure 9, where $h/l = 4$ and $Ro = 0{\cdot}1$. Figure 9(*a*) ($E = 10^{-6}$) gives the inviscid flow showing a strong, unattenuated wake for $H = 0{\cdot}4$. Figure 9(*b*) ($E = 10^{-3}$) shows the flow pattern when Ekman pumping (with scale $10l$) dominates internal dissipation (of scale $40l$). Near the obstacle the attenuation of the wake occurs at the horizontal boundaries but spreads into the centre of the container by the downstream distance $lHE^{-\frac{1}{2}}$. Since H is small, Ekman pumping is a zeroth-order effect even though $Re \gg Ro^{-1}$. The parameters in this example are typical of relatively inviscid small-Rossby-number geophysical flows whose depth h is large compared to l but small compared to l/Ro. For even shallower flows, where $h/l \sim 1$, the z-independent ($n = 0$) mode dominates the solution. It is unaffected by internal dissipation, and decays on the scale $\mu^{-1}l$. The other modes give vertical shear-layer contributions at topographic discontinuities, and the solution reduces to the vertical columnar disturbance discussed by Boyer (1971*a*, *b*).

† In three-dimensional flow past isolated topography an inviscid wake is unattenuated only if the flow is confined in a channel of finite cross-sectional area.

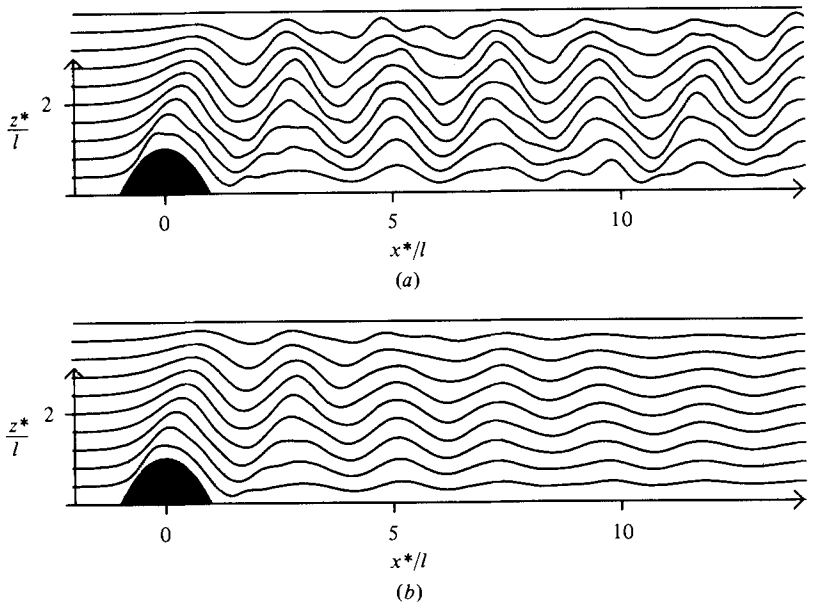

FIGURE 9. Finite-depth ($h/l = 4$, $\alpha = 1$) flow over the parabolic ridge f_2 at $Ro = 0{\cdot}1$: (a) inviscid ($E = 10^{-6}$); (b) viscous ($E = 10^{-2}$).

5. Wave drag

Downstream momentum transported by the inertial-wave wake subjects a submerged obstacle to a wave drag whose magnitude estimates the strength of the wake. Experimental results and a discussion of the horizontal force on submerged obstacles are given by Mason (1975), who concludes that the force is of magnitude $2\Omega\rho U\mathscr{V}$ (where $\mathscr{V}$ is a volume depending on obstacle shape and size) and direction relative to the oncoming flow depending on the Hide (1961) parameter α/H. For a given slope and small H, the obstacle behaves as a region of distributed vorticity. The force is transverse to the flow direction at infinity, i.e. a 'lift' force, and wave drag is zero. As H increases, the component of the force in the direction of the flow increases.

A difficulty arises in the consideration of drag on a ridge of given slope as $H \to 0$. In the neighbourhood of the ridge the approaching flow turns through an angle in the horizontal plane of Arctan $(\mathscr{A}/H)$, where $\mathscr{A}$ is the cross-sectional area of the ridge. The drag per unit width thus becomes infinite as $H \to 0$ for α finite, unless the flow approaches in such a way as to pass symmetrically over the ridge. Smith (1979) points out that symmetric flow occurs when the ridge is the central section of elongated isolated topography and the drag is regarded as the force in the direction of the flow far upstream (which is not necessarily normal to the ridge). In order to facilitate comparison with three-dimensional results (where the depth-independent zeroth-order mode makes no contribution to the drag), and to concentrate on inertial wave effects, only the drag due to the wake is considered in this section. This corresponds to considering the drag per unit width on the central section of elongated topography or to symmetric flow over a ridge. The drag per unit width is given by

$$2\rho\Omega h_0 l \int_{-\infty}^{\infty} p\Big|_{z=0} \frac{\partial f}{\partial x}\, dx. \tag{5.1}$$

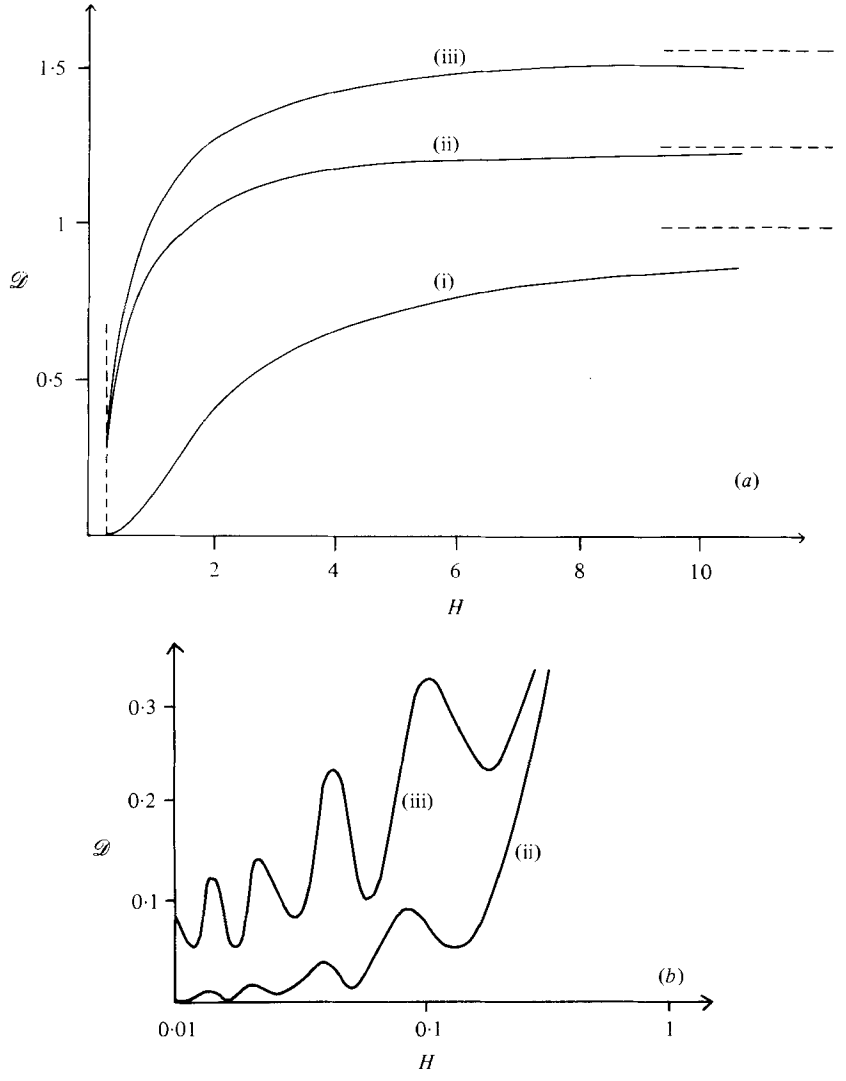

FIGURE 10. (*a*) The non-dimensional drag versus $H = hRo/l$ for (i) the Gaussian ridge, f_1; (ii) the parabolic ridge, f_2; (iii) the semicircular ridge, f_4. The dashed horizontal asymptotes give the drag in infinite depth flow. (*b*) As in (*a*) but with logarithmic scale for H.

From (2.4), (2.6) and (4.1), the pressure on the lower boundary to lowest order in the Rossby number, is given by

$$p = \frac{\alpha}{2\pi}\int_{-\infty}^{\infty} \hat{f}(k)\cot Hm e^{ikx}\,dk. \tag{5.2}$$

Thus the drag due to the inertial wave wake may be written $2\rho\Omega h_0^2\mathscr{D}$, where

$$\mathscr{D} = \frac{1}{2\pi i}\int_{-\infty}^{\infty} k[\hat{f}(k)]^2(\cot Hm - 1/Hm)\,dk. \tag{5.3}$$

This vanishes as $H \to 0$, and for deep flows

$$\mathscr{D} = \frac{1}{2\pi}\int_{-\infty}^{\infty} |k|\,[\hat{f}(k)]^2\,dk \quad (H \gg 1). \tag{5.4}$$

The infinite-depth drag is independent of the Reynolds number of the flow (to lowest order in the Rossby number): the amount of momentum transported away from the lower boundary is independent of the rate of decay of the disturbance.

For finite-depth inviscid flow (5.3) may be evaluated straightforwardly for even f using Cauchy's theorem. In the limit $Re \to \infty$

$$\mathscr{D} = \frac{1}{2\pi i}\int_{-\infty}^{\infty} k[\hat{f}(k)]^2 (\cot Hk^2 - 1/Hk^2)\, dk, \tag{5.5}$$

where the path of integration coincides with the real axis except in the neighbourhood of the poles at $k = \pm (n\pi/H)^{\frac{1}{2}}$, $n = \pm 1, \pm 2, \ldots$. As the corresponding poles at finite Reynolds number lie in the half-plane $\mathscr{I}k > 0$, the integration path for (5.5) is indented to pass below these singularities. Thus $\mathscr{D}$ is the sum of the Cauchy principal value of (5.5) and the contributions from the poles. For even f the integrand is odd, the principal value vanishes, and the sum of residues gives

$$\mathscr{D} = \frac{1}{H}\sum_{n=1}^{\infty} [\hat{f}((n\pi/H)^{\frac{1}{2}})]^2 \quad (Re \gg 1). \tag{5.6}$$

This reduces to (5.4) in the limit $H \to \infty$. For the obstacle f_1,

$$\mathscr{D} = \frac{\pi}{H}(\exp \pi/H - 1)^{-1} \tag{5.7}$$

$$\to \begin{cases} 1 - \frac{1}{2}\pi H^{-1} & \text{as} \quad H \to \infty, \\ \dfrac{\pi}{H}\exp\left(-\dfrac{\pi}{H}\right) & \text{as} \quad H \to 0. \end{cases}$$

The drag approaches a limiting value algebraically at large H and decays exponentially to zero as $H \to 0$. This behaviour is typical of any infinitely differentiable obstacle shape.

Figure 10 (a) gives the inviscid drag as a function of H for obstacles f_1, f_2 and the semi-circular cylinder: $f_4(x) = (1-x^2)^{\frac{1}{2}}$, $|x| < 1$; $f_4(x) = 0$, $|x| > 1$ (for which $\hat{f}_4(k) = J_1(k)/k$, where J_1 is the Bessel function of order one). The drag due to a top-hat ridge is infinite owing to the infinite amount of energy in the wake. For $H > 0{\cdot}3$ the drag increases monotonically to the infinite-depth value given by (5.4), which for f_2 is $4/\pi$ and for f_4 is $\frac{1}{2}\pi$. For a given obstacle height, the drag is greater for more abrupt topography. Moreover, the more rapid dispersion of the wake with height for abrupt topography means that the drag approaches its limiting value at shallower depths. For $H < 0{\cdot}3$ the dominant contribution to the drag comes from the first mode, and the sum in (5.6) may be approximated by its first term. The drag vanishes exponentially for f_1, as noted above. However, although the drag vanishes as $H \to 0$ for f_2 and f_4, the decrease is not monotonic. As $H \to 0$ the drag oscillates with increasing frequency but decreasing amplitude. Figure 10 (b) gives the drag as a function of H on a logarithmic scale. For f_4, $\mathscr{D}$ is of order $H^{\frac{1}{2}}$ for small H, and thus the drag can exceed 10 % of $2\Omega\rho h_0^2$ even for $H \simeq 0{\cdot}01$. From the drag on f_4, the drag on a circular cylinder with axis Oy^* confined between planes at $z^* = \pm h$ may be deduced. Since the flow field is symmetric about $z^* = 0$, the drag on the cylinder is twice that on f_4. Viscosity moves the pole corresponding to the first mode by $i\pi/2HRe$ (from (4.6)), and so the oscillatory variation of drag with Rossby number should be present in experiments where $Re \gg H^{-1}$. This is the case if $E \sim Ro^2$ and $h/l \gg 1$.

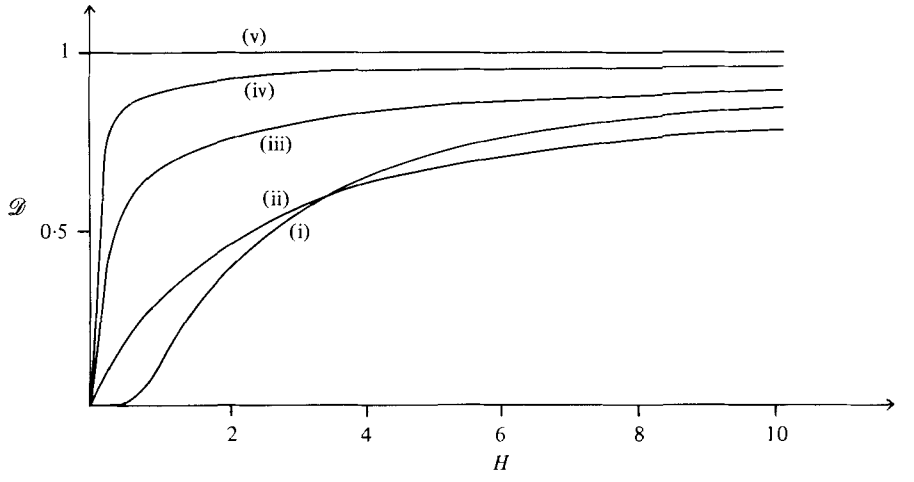

FIGURE 11. The non-dimensional drag versus $H = hRo/l$ for the Gaussian ridge, f_1, at various Reynolds numbers: (i) $Re = \infty$; (ii) 1; (iii) 0·1; (iv) 0·01; (v) 0.

Figure 11 gives the drag for the obstacle f_1 as a function of H for various viscosities. Increasing viscosity causes the disturbance to decay more rapidly downstream, and thus the effect on the drag of momentum reflected by the lower boundary decreases. The flow near the boundary resembles more closely infinite-depth flow, causing the drag to approach the infinite-depth value at smaller values of H. For highly viscous flow the drag has assumed over 50 % of its infinite-depth value by $H = 10Re$.

6. Discussion

Two-dimensional deep rotating flow over a ridge of finite slope has been shown to satisfy a linear field equation in the limit of vanishing Rossby number. The vertical flow structure is independent of whether the flow is regarded as an approximation to flow over the central portion of elongated three-dimensional topography or to flow over the central portion of a ridge confined in a wide channel. The horizontal structure varies with conditions at large cross-stream distances, and so in calculation of the drag on the topography attention is confined to the limit of elongated three-dimensional obstacles in a horizontally unbounded fluid.

The properties of the flow field may be conveniently described in terms of the obstacle-generated wave spectrum and its subsequent dispersion and dissipation. The amount of energy associated with a given wavenumber determines its importance in the motion and, for an energy spectrum with a distinct maximum, this may be parametrized by the upper and lower bounds k_u and k_l on the energetic wavenumbers, and by the wavenumber k_m corresponding to the maximum excited energy. Four vertical scales enter the problem: (i) the obstacle height h_0, which determines the size of the initial perturbation; (ii) $\pi l/k_m^2 Ro$, which determines the height over which the phase of the dominant disturbance changes by π; (iii) l/Ek_m^3, the vertical decay scale due to viscosity; and (iv) the fluid depth h. If h is smaller than $\pi l/k_m^2 Ro$ the phase of the maximum disturbance changes little over the fluid depth. If $H = hRo/l > \pi/k_m^2$ the disturbance phase changes significantly by the upper boundary, and so cannot be identified with a column. If h is smaller than l/Ek_m^3, viscosity does not damp the

disturbance before the upper boundary, and a reflected wave will be present. If $hE/l > k_m^{-3}$, viscosity causes the disturbance to decay before reaching the upper boundary. Dispersion causes the amplitude of the motion to decay algebraically with height even for inviscid flows. Thus a container will be effectively infinite when $[(k_u - k_l)\, hRo/l]^{-\frac{1}{2}} \exp[-k_m^3\, hE/l]$ is small.

The horizontal wavelength of the motion is determined by the obstacle width l, independently of the container depth. However, other horizontal scales of the motion vary with H. For $H \geqslant O(1)$ the two additional scales are (i) $l/(Re^{-1} + \mu)$, the viscous decay scale, and (ii) $4k_m Hl$, the distance to the first reflection of the disturbance from the lower boundary, and thus the distance over which a discussion in terms of wave propagation is useful. For inviscid infinitely deep flow, the downstream decay of the wake at fixed height is governed by the behaviour of the transform of the obstacle shape at large values of its argument: the smoother the topography, the more rapid the decay. For inviscid flow in containers of large but finite depth the amplitude of the wake at $x > 4k_m Hl$ is independent of x and proportional to $H^{-\frac{1}{2}}$. The disturbance energy carried past any fixed downstream station is constant. The flow consists of an infinite number of vertical modes whose relative importance is determined by the obstacle-shape transform.

For $H \leqslant O(1)$ a description in terms of wave propagation is useful solely for the upstream edge of the disturbance. Downstream from the obstacle a description in terms of vertical modes is more convenient – the shallower the flow, the fewer modes required. The horizontal scales of the motion, in addition to l, are then the viscous decay scales for internal dissipation, i.e. $lHRe$, and for Ekman pumping, i.e. $lHE^{-\frac{1}{2}} = lRoE_v^{-\frac{1}{2}}$, with the latter effect dominating whenever $Re \gtrsim O(Ro^{-1})$, and being of zeroth order provided $h/l \lesssim O(Ro^{-\frac{1}{2}})$.

No experimental results for flow over long ridges in deep containers are available for direct comparison with the solutions presented here. However, the series of three figures given by HIL for flow at various Rossby numbers over a sphere in a tank where $h/l = 12$ may be expected to manifest the gross features discussed above. At the experimental viscosity, $E = 1{\cdot}36 \times 10^{-3}$, the viscous scale height l/E is much larger than the tank depth, and so the disturbance is not viscously attenuated by the upper boundary. For figures 3(*a*, *b*) of HIL, where $Ro = 0{\cdot}2$ and $0{\cdot}09$ respectively, the Reynolds number of the flow is much larger than Ro^{-1}, and Ekman pumping on a scale of $E^{-\frac{1}{2}}l$ is the dominant viscous effect. In figure 3(*c*) of HIL ($Ro = 0{\cdot}034$) $Re \sim Ro^{-1}$, and internal dissipation is also important. The closest comparison with numerical results occurs at slightly larger values of the viscosity ($E = 10^{-2}$). A possible explanation may be found by noting that the sphere is of finite cross-stream extent, and thus strong cross-stream variations are present (e.g. figure 4(*b*) of HIL). The wake is weaker and disperses more rapidly both horizontally and vertically than the disturbance caused by a cylinder of the same diameter; thus downstream decay is enhanced.

The flow of figure 3(*a*) of HIL may be compared with that of figure 7(*b*) here. The first upward maximum of displacement shows the two effects of dispersion – the general tilt and a significant decay by $z^* \simeq \frac{2}{3}h$. Whether a second, weak, maximum occurs near the top of the tank cannot be decided from the observations. The flow of figure 3(*b*) of HIL is comparable with that of figure 6(*b*) here, although the inclusion of a solid boundary at $z^* \simeq 12l$ would reflect a small amount of energy. The figures

show a similar tilt and spread with height and neither manifests a second maximum. The flow of figure 3(*c*) of HIL corresponds to a flow of viscosity intermediate to those of figures 8(*b*, *c*) here, but more closely resembles that of figure 8(*c*), with little disturbance apart from the lifted flow almost directly above the obstacle. Since the tilt of the disturbance is determined experimentally by the position of the first upward maximum, which is in turn determined by the low-wavenumber components of the disturbance, those least affected by viscosity, Lighthill's inviscid theory gives a close description of this feature of these relatively viscous flows.

The radiation of inertial waves causes a drag which approaches a constant algebraically as $H \to \infty$, and decays to zero as $H \to 0$ in a manner determined by the obstacle shape transform at large values of its argument. The inclusion of viscosity causes the drag to approach its infinite-depth value at smaller values of H.

It is a pleasure to thank Professor Stewartson for introducing me to his work on deep rotating flows and suggesting consideration of viscous effects. This work also benefitted from the comments of the referees, one of whom suggested calculation of the drag.

REFERENCES

BOYER, D. L. 1971*a* Rotating flow over long shallow ridges. *Geophys. Fluid Dyn.* **2**, 165–184.

BOYER, D. L. 1971*b* Rotating flow over a step. *J. Fluid Mech.* **50**, 675–687.

CHENG, H. K. 1977 On inertial wave and flow structure at low Rossby number. *Z. angew. Math. Phys.* **28**, 753–769.

CHENG, H. K. & JOHNSON, E. R. 1982 Inertial waves above topography in an unbounded, rapidly rotating fluid. *Proc. R. Soc. Lond.* (in press).

HIDE, R. 1961 Origin of Jupiter's Great Red Spot. *Nature* **190**, 213–218.

HIDE, R., IBBETSON, A. & LIGHTHILL, M. J. 1968 On slow transverse flow past obstacles in a rapidly rotating fluid. *J. Fluid Mech.* **32**, 251–272.

HOCKING, L. M., MOORE, D. W. & WALTON, I. C. 1979 The drag on a sphere moving axially in a long rotating container. *J. Fluid Mech.* **90**, 781–793.

HUPPERT, H. E. 1975 Some remarks on the initiation of inertial Taylor columns. *J. Fluid Mech.* **67**, 397–412.

HUPPERT, H. E. & STERN, M. E. 1974 Ageostrophic effects in rotating stratified flow. *J. Fluid Mech.* **62**, 369–385.

INGERSOLL, A. P. 1969 Inertial Taylor columns and Jupiter's Great Red Spot. *J. Atmos. Sci.* **26**, 744–752.

LIGHTHILL, M. J. 1967 On waves generated in dispersive systems by travelling forcing effects, with applications to the dynamics of rotating fluids. *J. Fluid Mech.* **27**, 725–752.

MASON, P. J. 1975 Forces on bodies moving transversely through a rotating fluid. *J. Fluid Mech.* **71**, 577–599.

MASON, P. J. & SYKES, R. I. 1981 A numerical study of rapidly rotating flow over surface-mounted obstacles. *J. Fluid Mech.* **111**, 175–195.

MOORE, D. W. & SAFFMAN, P. G. 1968 The rise of a body through a rotating fluid in a container of finite length. *J. Fluid Mech.* **31**, 635–642.

MOORE, D. W. & SAFFMAN, P. G. 1969 The structure of free vertical shear layers in a rotating fluid and the motion produced by a slowly rising body. *Phil. Trans. R. Soc. Lond* A **264**, 597–634.

QUENEY, P. 1947 The problem of air flow over mountains: a summary of theoretical studies. *Bull. Am. Met. Soc.* **29**, 16–26.

SMITH, R. B. 1979 Some aspects of quasi-geostrophic flow over mountains. *J. Atmos. Sci.* **36**, 2385.

STEWARTSON, K. & CHENG, H. K. 1979 On the structure of inertial waves produced by an obstacle in a deep, rotating container. *J. Fluid Mech.* **91**, 415–432.

WHITHAM, G. B. 1974 *Linear and Nonlinear Waves*, chap. 11. Wiley.